Korean Journal of Chemical Engineering (2024) 41:2675–2689
https://doi.org/10.1007/s11814-024-00219-w

ORIGINAL ARTICLE

Phase Equilibria of Binary Mixtures of 3-Chloro-2-Hydroxypropyl Methacrylate and 2-N-Morpholinoethyl Methacrylate in Supercritical Carbon Dioxide

Divya Baskaran[1] · Cheol-Woong Park[1] · Uma Sankar Behera[1] · Hun-Soo Byun[1]

Received: 10 June 2024 / Revised: 2 July 2024 / Accepted: 4 July 2024 / Published online: 14 July 2024

Abstract
This study presents exceptional perception into the phase transition behavior of binary mixtures containing 3-chloro-2-hydroxypropyl methacrylate (3C2HM) or 2-N-morpholinoethyl methacrylate (2NMEM) in supercritical CO_2 at different operating temperatures (313.2–393.2 K) and pressures (3.36–33.90 MPa). The findings are expected to significantly contribute to the evolution of advanced materials and technologies in several industrial sectors. As temperature increases at constant pressure, carbon dioxide (CO_2) solubility in the monomer aqueous phase decreases. However, the solvability of the binary systems improved with temperature and mole fraction at steady pressure. The 2NMEM component exhibited higher polarizability and lower surface tension than the 3C2HM monomer, making it less soluble in CO_2, which is a nonpolar compound. The solution phase of the binary systems exhibited Type I phase behavior, and the phase diagrams were nearly identical. The experimental solubility data were adequately correlated with the Peng–Robinson equation of state with the aid of molecular interaction parameters (IPs) which was evaluated at 353.2 K. The optimized molecular IPs were nearly zero, confirming that both binary systems were nearly ideal mixture systems as the temperature increased. The model precision was evaluated by calculating the percentage of root-mean-square deviation (RSD%) at five temperatures using the molecular IPs. The calculated RSD% of the CO_2 + 3C2HM and CO_2 + 2NMEM systems were 4.70% and 4.91%, respectively, indicating that the model values fit reasonably well. Therefore, the predicted phase behavior agrees well with the experimental phase transitions of both systems. The characteristics of the critical solution curve were simulated to realise the interactions and transition behavior of the studied binary systems. This is the first study to demonstrate the solubility of CO_2 + 3C2HM and CO_2 + 2NMEM chemical mixtures, and it will be significant for chemical industries.

Keywords Monomer · Carbon dioxide · Solubility · Phase transition behavior · Peng–Robinson equation of state

Introduction

Supercritical fluid (SCF) technology is a promising environmentally friendly technology that has been in commercial use since the 1970s [1]. This technology has been significantly used for various purposes, such as extraction, crystallization, purification, precipitation, chemical reactions, product fractionation, fiber dyeing, powder formation, crystal growth, treatment of contaminated solids, and the development of microparticles and nanoparticles [2–4]. A fluid is considered supercritical when its pressure and temperature exceed their respective critical points. SCFs have dense and highly compressible properties that allow them to behave as either a liquid or a gas despite being neither. The liquid and gas phases of SCFs are identical and homogeneous in the critical region; hence, these fluid substances exhibit a liquid-like density, gas-like viscosity, and diffusivity, allowing for good mixing and mass transfer [5, 6]. For example, liquid characteristics allow for polymer plasticization, material solubilization, and extraction processes. The SCF technology can be divided into three classes depends on the

Divya Baskaran and Cheol-Woong Park have contributed equally to this work.

✉ Hun-Soo Byun
hsbyun@jnu.ac.kr

[1] Department of Chemical and Biomolecular Engineering, Chonnam National University, Yeosu, Jeonnam 59626, South Korea

solute present in the supercritical solvent: SCFs used as good solvents, SCFs used as antisolvents, and SCF-assisted spray drying.

Furthermore, it should be noted that SCFs possess unique thermo-physical properties. Notably, the critical pressure and temperature values of SCFs increase in proportion to the molecular weight, intermolecular hydrogen bonding, or polarity of the fluids. Such characteristics may be particularly important in various business and academic settings where the properties of SCFs are being studied or utilized. The expansion of pressure enlarges the density of SCFs without the raising viscosity, thus the solvation power increases at the supercritical range [7]. Some commonly reported SCFs include water, carbon dioxide (CO_2), ionic liquids, xenon, methane, ethane, propane, nitrous oxide, sulfur hexafluoride, trifluoromethane, and acetone. Although xenon and sulfur hexafluoride have low critical temperatures and pressures, they are not widely used for commercial applications because of their high production cost [8]. CO_2 is widely considered the most suitable SCF option because of its low critical points (7.38 MPa and 304.2 K), solubility parameter (7.5 cal/cm^3), nonflammability, nontoxicity, heat sensitivity, inertness, low cost, easy recyclability, and inability to leave residues after the process [9]. CO_2 is particularly useful for replacing toxic industrial solvents, and it is economically advantageous for liquid extraction and distillation methods related to various industrial activities performed in food and pharmaceutical industries [10]. Currently, considerable research is being conducted to study the solubility of monomers using SCF technology.

Monomers are simple molecules that can have varying lengths of molecular units covalently bonded to a core protein in their chemical structure. They play a crucial role in forming complex polymers that are essential in producing clothing, floor coverings, packaging, disposable plastic bags, paint, Teflon-coated cookware, fiberglass, and other items [11]. Methacrylate monomers are particularly versatile and are widely used in plastics, polymers, coatings, paints, adhesives, sealants, dental materials, medical adhesives, bone cement, resin, inks, printing materials, coated fabrics, electronics, and art and sculpture. The reason behind in the vast application is that their distinct fruity odor and unique properties including transparency, durability, and ease of polymerization [12, 13]. The evolution of the behavior of new methacrylate monomers is merely important in polymer science. Therefore, 3-chloro-2-hydroxypropyl methacrylate (3C2HM) and 2-N-morpholinoethyl methacrylate (2NMEM) monomers were investigated for the first time in the present research. Typically, 3C2HM monomer compounds are synthesized by employing an alkaline catalyst in the reaction between epichlorohydrin and methacrylic acid. This reaction yields the desired monomer compound [14, 15]. The reason behind its high thermal stability is the presence of a strongly cross-linked matrix as well as the beta position of the quaternary group contains a hydroxyl group. This hydroxyl group stabilizes the C–N bond through its − I and + M effects [16]. However, 3C2HM is expensive and toxic, making it difficult to handle, even though its concentration can be minimized for industrial applications [17].

The use of monomers is essential in the production of acrylic polymers, which are used in various applications such as adhesives, printing inks, coatings, pharmaceuticals, agrochemicals, and dyestuffs. Monomers are also used as reactive diluents and as an alternative to styrene in unsaturated polyester [18]. One of the cationic monomers, 2NMEM, has a copolymer with a highly hydrophilic nature due to the presence of tertiary amine and heterocyclic oxygen with an active hydroxyl group [19]. Generally, 2NMEM is a compound that contains an active polymer compound. This active polymer compound is synthesized through the acylation of N-morpholinoethanol with either methacryloyl chloride or methacrylic acid anhydride [20]. This comonomer is used in pharmaceuticals, polymer films, dentin adhesive formulation control, and other applications [21]. Both the 3C2HM and 2NMEM polymer components can be used to create biocompatible, nontoxic, and multi-stimuli-responsive polymers because of their high reactivity. To offer various industrial recommendations, it is important to have a clear understanding of the phase performance of 3C2HM and 2NMEM monomers across various ranges of operating conditions. CO_2 as an SCF is an eco-friendly solvent, and its solvation power has a great impact on the investigated methacrylate monomers.

Researchers have documented extensive phase behavior data on binary mixtures of different monomers in CO_2 SCF [22–24]. Lora and McHugh [25] studied the P vs. x isotherms of a methyl methacrylate–CO_2 system and used the Peng–Robinson (P-R) equation of state (EOS) and the statistical associating fluid theory (SAFT) EOS to model the system at different temperatures of 26–170 °C and pressures as high as 2500 bar. Byun and Lee [26] recorded the solubility data of benzyl acrylate + CO_2 and benzyl methacrylate + CO_2 systems at a high pressure of 24.43 MPa for different isotherms. Cho et al. [27] investigated the vapor–liquid equilibria (VLEs) for a tetrahydrofurfuryl methacrylate + CO_2 system at wide ranges of temperature (313.2–393.2 K) and pressure (≤ 22.07 MPa). Dhamodharan et al. [28] studied the solubility statistics of fluoromonomer (meth) acrylates in a CO_2 SCF solvent under a high-pressure range of 3.31–16.84 MPa. In other previous studies, computation modeling was predicted using the P-R EOS, and experimental validations were performed for methacrylate binary systems such as 2-(diisopropylamino) ethyl methacrylate + CO_2 [29] and 2-(diethylamino) ethyl acrylate + CO_2 and 2-(diethylamino) ethyl methacrylate [30] under pressurized conditions. Therefore, this study aims to

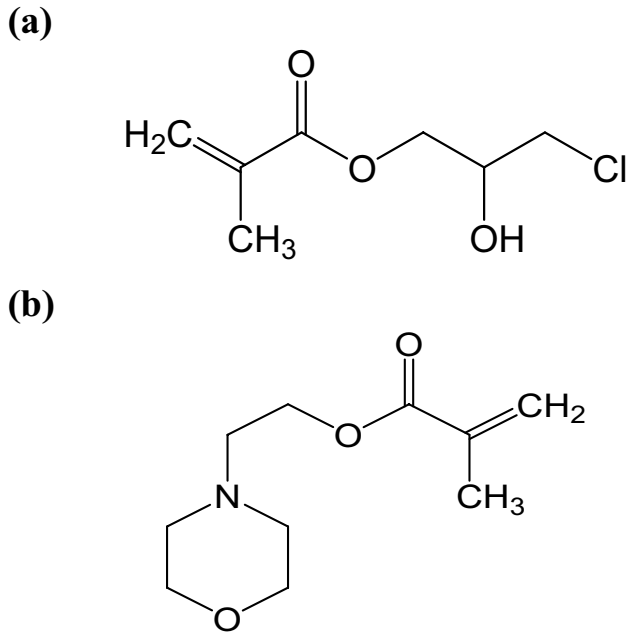

Fig. 1 Chemical configurations of **a** 3-chloro-2-hydroxypropyl methacrylate, and **b** 2-*N*-morpholinoethyl methacrylate

further extend the research by studying the equilibrium solubility and predicting the theoretical model of new methacrylate monomers in CO_2.

The constitutional aim of this research endeavor was to inspect how the polymer components of 3C2HM and 2NMEM behave in supercritical CO_2 at different temperatures and pressures. The study investigated correlations between the data modeled using the P-R cubic EOS with optimized molecular interaction parameters (IPs) and the experimental results for both methacrylate binary systems. The effect of temperature on the energy parameters was also examined to reduce the percentage of root-mean-square deviation (RSD%) and improve the accuracy of the predicted data. Additionally, the critical solution curve was characterized, and the critical properties and vapor pressure of the pure components were evaluated using the group contribution method.

Materials and Methods

Materials

The 3C2HM ($H_2C=C(CH_3)CO_2CH_2CH(OH)CH_2Cl$; CAS RN 13159-52-9; mass fraction: > 0.965) and 2NMEM ($H_2C=C(CH_3)CO_2(CH_2)_2C_4H_8NO$; CAS RN 2997-88-8; mass fraction: > 0.950) components required for this study were purchased from Sigma-Aldrich. Figure 1 illustrates the chemical component configuration of 3C2HM and 2NMEM. The CO_2 gas cylinder was supplied by the dealer of Deokyang Gases Co. Ltd. All chemical components and gases were used as purchased. Table 1 summarizes the chemical specification of the pure components for the experimental study. Table 2 presents the thermodynamic properties (molecular weight, boiling temperature, critical pressure, critical

Table 1 Specification of the chemicals used in this study

Chemical name	Source	Purity[a]	Purification method	Analysis method[a]
CO_2	Deokyang Gases Co. Ltd	> 0.999	None	–
3-Chloro-2-Hydroxypropyl Methacrylate	Sigma-Aldrich (CAS RN 13159–52-9)	> 0.965	None	GC[b]
2-*N*-Morpholinoethyl Methacrylate	Sigma-Aldrich (CAS RN 2997–88-8)	> 0.950	None	GC[b]

[a]Both the analysis method and the mass fraction purity were provided by the suppliers

[b]GC Gas–liquid chromatography

Table 2 The properties of pure component of carbon dioxide (CO_2), 3-chloro-2-hydroxypropyl methacrylate (3C2HM) and 2-*N*-morpholinoethyl methacrylate (2NMEM)

Compounds	M_w	Chemical structure	T_b/K	T_c/K	P_c/MPa	ω
CO_2	44.01	O=C=O		304.2	7.38	0.225
3C2HM	178.61	$H_2C=C(CH_3)CO_2CH_2CH(OH)CH_2Cl$	560.6[a]	776.9	3.45	0.701
2NMEM	199.25	$H_2C=C(CH_3)CO_2(CH_2)_2C_4H_8NO$	564.9[a]	772.6	2.79	0.678

M_w molecular weight, T_b boiling temperature, T_c critical temperature, P_c critical pressure, ω acentric factor

[a]ChemSpider

temperature, and acentric factor of the pure components of CO_2, 3C2HM, and 2NMEM.

Phase Behavior Recording Set-up and Experimentation

This study aimed to deduce the phase diagram of two-component systems, namely, CO_2 + 3C2HM and CO_2 + 2NMEM, using a high-pressure static apparatus and a synthetic method. The laboratory setup and operating conditions have been previously described in detail [31, 32]. The measuring instrument for the phase behavior consists of three main sections: a variable-volume view cell (3 V cell), a pump-connected high-pressure generator (HPG), and a data display (DD) system. The 3 V cell is made of nickel with austenitic steel, and it has an inner dia of 1.59 cm, an outer dia of 5.7 cm, and a volume of 28 cm^3. The 3 V cell can allow an elevated pressure of 70 MPa, and it is used to study the phase transitions such as bubble point (BLP) dew point (DWP) and critical point (CLP) of binary solution systems. The total pressure of the instrument is recorded by the HPG (Model 37–5.75–60), while the inside pressure of the 3 V cell is analyzed by a Heise gauge (Model CM-53920, Dresser Ind, $0 \le P \le 34$ MPa). The inner temperature of the 3 V cell is proportioned by a platinum resistance thermometer (Thermometric Corp., Class A, standard uncertainty (u): ± 0.20 K) and measured by a digital multimeter (Model 7563, Yokogawa). The phase transition of the reaction mixtures inside the cell is displayed through the DD system, which uses a borescope camera (Olympus Corp., Model: WAT-202B, Version: F100-038-000-50) to display the video of the phase transition. A sapphire window (thickness: 1.9 cm) is located opposite the 3 V cell section to discover the solution phase behavior (Fig. 2).

The empty 3 V cell was purged with N_2 and CO_2 gases several times to remove trace quantities of foreign materials and residual air. Thereafter, a syringe was used to load the 3 V cell with appropriate amounts of the 3C2HM and 2NMEM monomers within $u = \pm 0.0008$ g, and CO_2 was added using a high-pressure bomb within $u = \pm 0.002$ g. The pressure inside the 3 V cell was altered by moving a rotatable piston (size: 2.54 cm) using a water pressurizer. The mixture composition was determined using the weight. The 3 V cell was heated to attain a one-phase region. After achieving the monophase in the reaction cell, the same condition was maintained for 30 min. A magnetic stir bar is essential for mixing the pure components and clearly visualizing the mixture. The borescope camera was used to transmit light into the 3 V cell, and a fiber optic cable was connected to a high-density illuminator (Model 180) to improve the vibrancy of the view. Here, the pressure was gradually reduced by regulating the piston to reach the different BLP, DWP, and CLP phase conditions.

Opalescence may be observed within the reaction cell at the point of criticality (LV), where the liquid and vapor densities are equivalent. This phenomenon can be attributed to the refractive index of the medium changing as it approaches the critical point, which results in light scattering. The critical point is a crucial parameter in thermodynamics, and its prediction is of utmost importance in industrial applications, such as chemical engineering, oil and gas production, and material science [33, 34]. Additionally, adjusting the pressure and temperature will result in different points of tiny bubble formation, followed by the appearance of mist clusters in the cell; these points are referred to as bubble

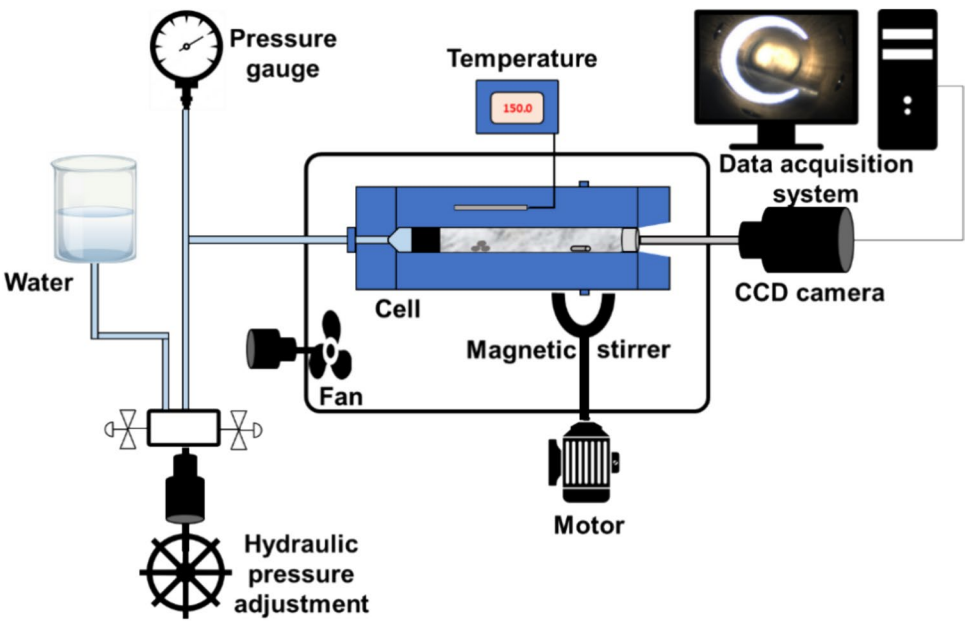

Fig. 2 Schematic representation of the experimental apparatus set-up of the high-pressure system used in the study [31, 32]

point (L→LV) and dew point (L→LV), respectively [35, 36]. The composition of the overall mixture is equivalent to that of the respective phase even though they appear as BLP and DWP. In the second phase, the mass of the pure component can be considered negligible. The process for obtaining a VLE dataset involves changing the temperature and pressure of the system. This process must be repeated three times to achieve the desired '*u*'. Finally, the average numerical values can be identified by excluding the maximum and minimum values from the dataset. In this study, the solution co-existence space of the CO_2 + 3C2HM and CO_2 + 2NMEM systems was inquired at temperatures of 313.2, 333.2, 353.2, 373.2, and 393.2 K; elevated pressures of $3.25 \le P \le 33.90$ MPa; and various mole fractions of $0.0560 \le x \le 0.7925$. According to the supplier, the maximum '*u*' in the temperature, pressure, and mole fraction of the monomers was ± 0.20 K, ± 0.05 MPa, and ± 0.0008, which were used for all the experiments.

Application of P-R *EOS* Correlation in the Prediction of Phase Behavior

The thermodynamic model of the solution phase equilibria for the CO_2 + 3C2HM and CO_2 + 2NMEM binary systems was deduced using the P-R correlation with the van der Waals one-fluid mixing rule. Many reports have confirmed that the P-R EOS correlation is one of satisfactory EOS that can represent the phase behavior of pure component fluids [37]. The VLE data was predicted by adjusting or optimizing the molecular IPs of the P-R EOS correlation. It appears that the pure component properties of 3C2HM and 2NMEM have not yet been covered in the literature. However, their critical constants, including critical temperature (T_c), boiling temperature (T_b), and critical pressure (P_c), have been predicted using the group contribution method proposed by Joback and Lydersen. Additionally, the vapor pressure of these components has been estimated using the Lee–Kesler approach [38–40]. The acentric factors (ω) are determined based on the critical properties (T_c and T_b) using the method proposed by Pitzer et al. [41]. Table 2 presents the physical properties used for the thermodynamic modeling of the VLE data of the binary system, which were used to optimize the IPs.

The P-R EOS correlation is

$$P = \frac{RT}{v-b} - \frac{a\alpha(T_r,\omega)}{v(v+b)+b(v-b)} \tag{1}$$

$$a = 0.45724\frac{R^2T_c^2}{P_c} \tag{2}$$

$$b = 0.07780\frac{RT_c}{P_c} \tag{3}$$

$$\alpha(T_r,\omega) = \left(1 + k\left(1 - T_r^{\frac{1}{2}}\right)\right)^2 \tag{4}$$

where a is the attraction factor [Pa m^6/mol^2], b is the co-volume factor [m^3/mol], R is the universal gas constant [8.314462 J/(mol K)], T is the experimental temperature [K], P is the experimental pressure [Pa], v is the molar volume [m^3/mol], T_r is the reduced temperature [K], α is polarizability [cm^3], ω is the acentric factor, and k is the acentric correction parameter, which is expressed as follows:

$$k = 0.37646 + 1.5422\omega + 0.26999\omega^2 \tag{5}$$

The mixing rule is summarized as follows:

$$a_{mix} = \sum_i \sum_i x_i x_j a_{ij} \tag{6}$$

$$b_{mix} = \sum_i \sum_i x_i x_j b_{ij} \tag{7}$$

$$a_{ij} = \left(a_{ii}a_{ij}\right)^{\frac{1}{2}}(1 - k_{ij}) \tag{8}$$

$$b_{ij} = \frac{1}{2}\left(b_{ii}+b_{ij}\right)(1 - \eta_{ij}) \tag{9}$$

where $k_{ij}=k_{ji}$, $k_{ii}=k_{jj}=0$, $\eta_{ij}=\eta_{ji}$, $\eta_{ii}=\eta_{jj}=0$, x_i is the mole fraction of the ith component in the liquid, a_i and b_i are the P-R EOS parameters of the *i*th pure substances, and k_{ij} and η_{ij} are the molecular energy and size parameter for the *i–j* pair, respectively. The objective function (OBF) and RSD% percentage are as follows:

$$OBF = \sum_{i=1}^{N}\left(\frac{P_{exp} - P_{cal}}{P_{exp}}\right)^2 \tag{10}$$

$$RSD\,(\%) = \frac{100}{N}\sum_{i=1}^{N}\frac{\left|P_i^{cal} - P_i^{exp}\right|}{P_i^{exp}} \tag{11}$$

where N represents the number of the experimental VLE data, and *exp* and *cal* denote the experimental and calculated bubble point pressures, respectively. The least-squares approach was used in PYTHON programming along with Marquardt's method to solve and minimize the OBF [42]. The RSD% was evaluated by adjusting the IPs and investigating the effect of temperature on energy and key parameters. The thermodynamic properties of the binary mixture were predicted using the P-R EOS correlation with the IPs of k_{ij} and η_{ij}.

Results and Discussion

Assessment of the Solution Phase Equilibria

The *P*–*x* isotherms of the two-component systems, CO_2 + 3C2HM and CO_2 + 2NMEM, were examined at five different temperatures and various pressures using the mole fraction of the monomers in the mixtures. The systems were studied at different phase transitions (BLP, DWP, and CLP), and the measurements were recorded at thrice with the spec of reproducibility: $u(P) = \pm 0.05$ MPa and $u(T) = \pm 0.20$ K. In both experiments, the phase behavior was investigated over wide temperature ($313.2 \le T \le 393.2$ K), pressure ($3.25 \le P \le 33.90$ MPa), and mole fraction ($0.0560 \le x \le 0.7925$) ranges. The maximum error was found to be ± 1.01% with respect to the values of two independent phase transition points. This study provides novel perception into the transition behavior of CO_2 + 3C2HM and CO_2 + 2NMEM systems. It also elucidates previously unknown properties and interactions of these systems.

CO_2 + 3C2HM System

Table 3 presents the measured VLE dataset of the CO_2 + 3C2HM ($(1-x)$ $CO_2 + x$ $H_2C=C(CH_3)CO_2CH_2CH(OH)CH_2Cl$) system. The isotherm of the binary solution phase (*P*–*x*) was recorded at range of temperatures ($313.2 \le T \le 393.2$ K), elevated pressures ($3.36 \le P \le 33.90$ MPa), and mole fractions ($0.1002 \le x \le 0.7925$). The VLE dataset comprised 75 data points, with each temperature, that is, 313.2 K, 333.2 K, 353.2 K, 373.2 K, and 393.2 K, having 15 data points. The results revealed that there was only one CLP pressure transition and 74 BLPs for the system, indicating that there were no three-phase regions recorded for the system within the specified temperature range. Surprisingly, no DWP pressures were observed, and only one single-phase transition was recorded at *T*, *P*, and *x* values of 393.2 K, 33.90 MPa, and 0.1002, respectively. Therefore, the system had a total of 74 liquid-to-vapor phase transitions and 1 liquid–vapor phase transition across a range of process conditions during the measurement of the solution coexistence space of the 3C2HM component in CO_2 solvent.

Figure 3a shows plots of the experimental isotherms of pressure versus composition (*P* vs. *x*) for the CO_2 + 3C2HM system at various temperatures and elevated pressures. The graph shows that the solubility of supercritical CO_2 in the 3C2HM monomer aqueous phase decreases as temperature increases but increases as pressure increases. Therefore, it is worth noting that at constant pressure, the solubility of

Table 3 Experimental data for the supercritical CO_2 + 3-chloro-2-hydroxypropyl methacrylate (3C2HM) [x $H_2C=C(CH_3)CO_2CH_2CH(OH)CH_2Cl + (1-x)$ CO_2] system in this work

3C2HM mole fraction	P^a/MPa	Transition[b]
***T*[a]/K = 313.2**		
0.1002	16.35	BLP
0.1757	14.82	BLP
0.2001	14.35	BLP
0.2537	12.35	BLP
0.3038	10.81	BLP
0.3600	10.01	BLP
0.4189	8.86	BLP
0.4894	7.87	BLP
0.5125	7.33	BLP
0.5926	6.22	BLP
0.6428	5.30	BLP
0.6864	4.81	BLP
0.7183	4.40	BLP
0.7625	3.86	BLP
0.7925	3.36	BLP
***T*[a]/K = 333.2**		
0.1002	21.50	BLP
0.1757	19.65	BLP
0.2001	18.50	BLP
0.2537	16.84	BLP
0.3038	14.90	BLP
0.3600	13.48	BLP
0.4189	11.97	BLP
0.4894	10.11	BLP
0.5125	9.81	BLP
0.5926	8.13	BLP
0.6428	6.97	BLP
0.6864	6.28	BLP
0.7183	5.63	BLP
0.7625	4.93	BLP
0.7925	4.53	BLP
***T*[a]/K = 353.2**		
0.1002	26.87	BLP
0.1757	24.16	BLP
0.2001	23.10	BLP
0.2537	21.48	BLP
0.3038	19.28	BLP
0.3600	17.22	BLP
0.4189	15.38	BLP
0.4894	13.09	BLP
0.5125	12.52	BLP
0.5926	10.47	BLP
0.6428	9.03	BLP
0.6864	8.19	BLP
0.7183	7.52	BLP
0.7625	6.43	BLP
0.7925	5.83	BLP

Table 3 (continued)

3C2HM mole fraction	P^a/MPa	Transition[b]
***T*[a]/K = 373.2**		
0.1002	30.42	BLP
0.1757	28.88	BLP
0.2001	28.03	BLP
0.2537	26.28	BLP
0.3038	24.17	BLP
0.3600	21.90	BLP
0.4189	18.72	BLP
0.4894	15.90	BLP
0.5125	15.24	BLP
0.5926	12.76	BLP
0.6428	10.90	BLP
0.6864	9.42	BLP
0.7183	8.84	BLP
0.7625	8.00	BLP
0.7925	7.10	BLP
***T*[a]/K = 393.2**		
0.1002	33.90	CLP
0.1757	32.45	BLP
0.2001	31.61	BLP
0.2537	29.22	BLP
0.3038	26.61	BLP
0.3600	23.93	BLP
0.4189	21.22	BLP
0.4894	18.22	BLP
0.5125	17.32	BLP
0.5926	14.26	BLP
0.6428	12.30	BLP
0.6864	11.02	BLP
0.7183	9.86	BLP
0.7625	9.10	BLP
0.7925	8.10	BLP

[a]Standard uncertainties u are $u(T) = 0.20$ K, $u(P) = 0.05$ MPa and $u(x) = 0.0008$

[b]*BLP* is a Bubble-Point ($L \rightarrow$LV), *CLP* is a Critical-Point (LV), *V*-Vapor phase and *L*-Liquid phase

CO_2 tends to decrease as the temperature raises. Conversely, the solvability of the $CO_2 + 3C2HM$ system improves as the temperature raises at steady pressure. This increase in solubility is due to the weakening of the bonding strength between CO_2 and the 3C2HM monomer under high-temperature and high-pressure conditions, which contributes to an increase in the order of binary system solubility [43, 44]. Moreover, the nonpolarity characteristics of CO_2 can accelerate the dissolution of the monomer in the solvent since 3C2HM is a less polar component. At a maximum pressure of 33.90 MPa, a single-phase liquid–vapor phase transition was recorded at a minimum monomer composition of 0.1002. Thus, the solubility of the pure 3C2HM monomer

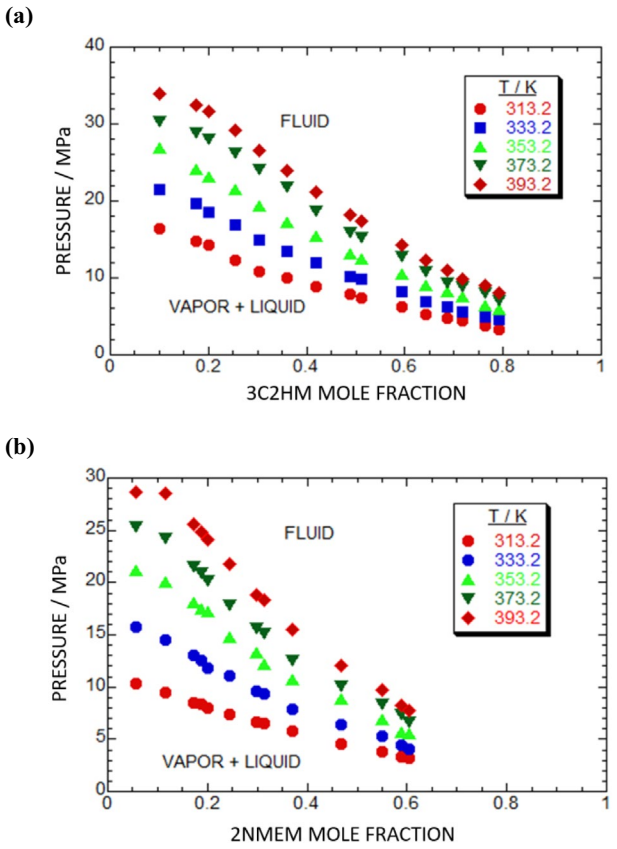

Fig. 3 Pressure *vs.* mole fraction plots comparing the experimental data (solid symbols) obtained in this work for the $CO_2 + 3C2HM$ $\{(1-x)CO_2 + x\ H_2C=C(CH_3)CO_2CH_2CH(OH)CH_2Cl\}$ **a** and $CO_2 + 2NMEM$ $\{(1-x)CO_2 + x\ H_2C=C(CH_3)CO_2(CH_2)_2C_4H_8NO\}$ **b** systems at temperatures of 313.2, 333.2, 353.2, 373.2, and 393.2 K. (●, 313.2 K; ■, 333.2 K; ▲, 353.2 K; ▼, 373.2 K; ◆, 393.2 K

component decreases as the composition of the monomer in supercritical solvent CO_2 increases. Finally, the critical point was observed at a high temperature of 393.2 K and an elevated pressure of 33.90 MPa. Here, the boiling point of the 3C2HM component (560.6 K) plays a pivotal role in the existence of the CLP, indicating the likelihood of mono phase at high-temperature and pressurized conditions. As shown in Fig. 3a, the single-phase region was discovered at the uppermost point of each isotherm, while the two-phase region was ascertained at the lowermost point of each isotherm. This phase behavior is consistent with the behavior of various binary systems [45, 46]. Furthermore, the phase transition behavior of the two-component $CO_2 + 3C2HM$ system is consistent with the simplest Type I category [47]. The one-phase region was exhibited throughout the phase diagram where the CLP pressure recorded at elevated conditions. Consequently, this phase diagram reveals that the solubility of the binary system is enhanced by increasing the temperature and pressure while decreasing the 3C2HM monomer composition [48, 49].

CO_2 + 2NMEM System

Table 4 presents the findings of the measured phase diagram dataset of the CO_2 + 2NMEM ((1 − *x*) CO_2 + *x* $H_2C=C(CH_3)CO_2(CH_2)_2C_4H_8NO$)) system. Like previous system, the isotherm (P–x) of this system was recorded at different temperatures ($313.2 \le T \le 393.2$ K), elevated pressures ($3.25 \le P \le 28.70$ MPa), and mole fractions ($0.0560 \le x \le 0.6037$). A total of 65 data points were collected, with five various temperatures having 13 data points each. The presence of 57 BLP, 6 DWP, and 2 CLP pressure transitions was observed during the measurement of the phase behavior. There were no three-phase regions in the system at the operating temperature ranges. However, two DWP phase transitions were observed at different pressures and five fixed temperatures (15.80 (333.2 K), 21.20 (353.2 K), 24.20 (373.2 K), 25.30 (373.2 K), 28.50 (393.2 K), and 28.70 (393.2 K) MPa). Additionally, two single-phase transitions of CLP pressures of 20.07 MPa and 20.86 MPa were observed at 353.2 K and 373.2 K, respectively. During the measurement, a total of 57 liquid-to-vapor two-phase transitions, 6 vapor-to-liquid two-phase transitions, and 2 liquid-to-vapor one-phase transitions were recorded under various process conditions.

Figure 3b presents the *P vs. x* isotherms for the CO_2 + 2NMEM system at different temperatures and elevated pressures. It is worth noting that the chemical solubility of CO_2 in the aqueous phase of the 2NMEM monomer decreases as the temperature increases at constant pressure, similar to the other system. However, the solubility of the CO_2 + 2NMEM system magnified as the temperature inflation at steady pressure. These observations can be useful in designing and optimizing systems that involve the use of the liquid phase of the 2NMEM monomer and CO_2. Moreover, the solubility of the pure 2NMEM monomer component decreases with a rise in the composition of the monomer in CO_2 solvent. According to Konynenburg and Scott's classification [50], it can be stated that this particular binary system displays Type I phase behavior. A mono-phase region was achieved at the top of each isotherm, while a two-phase region was achieved at the bottom of each isotherm. The single-phase region is a prevalent feature in the phase diagram of binary systems. At elevated pressure conditions, a critical point known as CLP appears, which is characterized by a particular pressure point. Moreover, an increase in temperature under pressurized conditions loosened the interaction bonding between CO_2 and the 2NMEM monomer, resulting in an extended chemical solubility of the mixture.

The 3C2HM monomer had a polarizability of 16.07 ± 0.5 10^{-24} cm^3 and surface tension of 36.6 ± 3.0 dyne/cm, whereas the 2NMEM component had high polarizability of 20.9 ± 0.5 10^{-4} cm^3 and low surface tension of 33.6 ± 3.0 dyne/cm. This caused 2NMEM to exhibit less

Table 4 Experimental data for the supercritical CO_2 + 2-*N*-morpholinoethyl methacrylate (2NMEM) [*x* $H_2C=C(CH_3)CO_2(CH_2)_2C_4H_8NO$ + (1–*x*) CO_2] system in this work

2NMEM Mole fraction	P^a/MPa	Transition[b]
***T*[a]/*K* = 313.2**		
0.0560	10.30	BLP
0.1156	9.52	BLP
0.1875	8.32	BLP
0.1722	8.55	BLP
0.2015	8.00	BLP
0.2432	7.33	BLP
0.2977	6.69	BLP
0.3130	6.49	BLP
0.3705	5.77	BLP
0.4684	4.58	BLP
0.5495	3.82	BLP
0.5888	3.37	BLP
0.6037	3.25	BLP
***T*[a]/*K* = 333.2**		
0.0560	15.80	DWP
0.1156	14.53	BLP
0.1875	12.59	BLP
0.1722	12.99	BLP
0.2015	11.76	BLP
0.2432	11.07	BLP
0.2977	9.64	BLP
0.3130	9.32	BLP
0.3705	7.93	BLP
0.4684	6.35	BLP
0.5495	5.35	BLP
0.5888	4.45	BLP
0.6037	4.07	BLP
***T*[a]/*K* = 353.2**		
0.0560	21.20	DWP
0.1156	20.07	CLP
0.1875	17.51	BLP
0.1722	18.09	BLP
0.2015	17.21	BLP
0.2432	14.76	BLP
0.2977	13.28	BLP
0.3130	12.14	BLP
0.3705	10.66	BLP
0.4684	8.83	BLP
0.5495	6.93	BLP
0.5888	5.72	BLP
0.6037	5.55	BLP
***T*[a]/*K* = 373.2**		
0.0560	25.30	DWP
0.1156	24.20	DWP
0.1875	20.86	CLP
0.1722	21.59	BLP
0.2015	20.16	BLP

Table 4 (continued)

2NMEM Mole fraction	P^a/MPa	Transition[b]
0.2432	17.87	BLP
0.2977	15.59	BLP
0.3130	15.08	BLP
0.3705	12.59	BLP
0.4684	10.14	BLP
0.5495	8.41	BLP
0.5888	7.41	BLP
0.6037	6.62	BLP
$T^a/K = 393.2$		
0.0560	28.70	DWP
0.1156	28.50	DWP
0.1875	24.90	BLP
0.1722	25.55	BLP
0.2015	24.07	BLP
0.2432	21.76	BLP
0.2977	18.88	BLP
0.3130	18.28	BLP
0.3705	15.50	BLP
0.4684	12.07	BLP
0.5495	9.76	BLP
0.5888	8.21	BLP
0.6037	7.79	BLP

[a]Standard uncertainties are $u(T) = 0.2$ K and $u(P) = 0.05$ MPa

[b]BLP is a Bubble point ($L \rightarrow$LV), *CLP* is a Critical point (LV), *DWP* is a Dew point (V $\rightarrow$VL), *V*-Vapor phase and *L*-Liquid phase

solubility in CO_2 than 3C2HM since CO_2 is a nonpolar compound. The 3C2HM component had a lower molar volume (151.7 ± 3 cm^3) than the 2NMEM component (190.5 ± 3 cm^3), confirming that the single-phase region appeared at lower temperatures (353.2 K and 373.2 K), lower pressure (20.07 MPa and 20.86 MPa), and higher compositions (0.1156 and 0.1875) of the monomer for the CO_2 + 2NMEM system. Similar effects may be caused by the small difference in molecular weight between the monomers [51, 52]. Obviously, the chemical solubility of the 2NMEM was less than that of the 3C2HM monomer in supercritical solvent CO_2, hence, the solubility existence space in the CO_2 + 2NMEM system was obtained at elevated pressure conditions. Additionally, the vapor curve was pulled down as the ω parameter increased, resulting in elevated BLP pressures; thus, the 3C2HM system (ω: 0.701) exhibited higher pressures in the *P*–*x* space than the 2NMEM system (ω: 0.678) [53]. However, the phase diagrams of the 3C2HM (CAS number 13159-52-9) and 2NMEM (CAS number 2997-88-8) systems were extremely similar and could be considered almost indistinguishable from one another. Changes in the chemical configuration of the monomer did not affect the phase diagram, but the interaction between CO_2 and the monomer affected the phase transition conditions. Based on our observations, we can infer that the miscibility of CO_2 in both binary systems declines as the temperature increases at constant pressure. This finding could assist in the evolution of mere implied separation processes involving the use of CO_2 solvent.

Thermodynamic Modeling Using the P-R *EOS* Correlation

The implication of EOS in characterizing the behavior of substances under varying temperature, pressure, and volume conditions is essential. The evolution of EOS, from the original van der Waals equation to the subsequent advancements by Redlich and Kwong, and later Soave with the introduction of the Soave–Redlich–Kwong (SRK) EOS. The SRK EOS model proved beneficial in accurately describing the vapor pressure of pure components in hydrocarbon systems, but poor liquid density prediction although it showed limitations in systems exhibiting upper or lower critical solution temperatures (UCST and LCST) [54]. The Peng-Robinson (P-R) EOS, renowned for its ability to predict the behavior of non-polar and polar fluids as well as its accuracy in handling a wide range of temperatures and pressures, emerged as a robust option for predicting VLE and guiding separation processes. This offers algebraic simplicity and generality since it requires minimal data. Its volume-translated counterpart, VT-PR EOS, demonstrated favorable results in predicting vapor pressures of nonpolar and polar pure fluids but posed limitations in directly applying to supercritical conditions for predicting VLE [55]. Additionally, the Statistical Associating Fluid Theory (SAFT) EOS and its SAFT-γ-Mie variation played significant roles in modeling vapor pressure and liquid density data, with the latter gaining attention for its proficient acetate ester prediction, despite limitations in modeling ester-alkaline binary VLE phase behavior and dipolar compound behavior [56]. The cubic-plus-association (CPA) EOS proved effective in correlating with the LLE for water-alkane systems, demonstrating its efficacy with a single interaction parameter. The choice of model depends on the specific application and the properties of the fluid being modeled. In the context of the study involving a less associated substance containing binary system (methacrylate + CO_2), the P-R EOS was chosen for modeling VLE due to its simplicity and reasonable accuracy compared to other EOS models.

In this study, the P-R EOS correlation and the van der Waals one-fluid mixing rule were extensively employed at five different temperatures and various pressures. A study was performed to determine the correlation between the VLE of the two binary systems: CO_2 + 3C2HM and CO_2 + 2NMEM. Molecular IPs were utilized to aid in this investigation.

Computation of the Phase Diagram by Adjusting the *IPs*

A theoretical computation of the P-R EOS was adequately applied to predict the transition behavior of the pure component binary system. Sect. "Application of P-R EOS correlation in the prediction of phase behavior" details the optimization of the molecular IPs with their correlation rules. Table 2 shows the T_c, T_b, P_c, and ω parameters for CO_2, 3C2HM, and 2NMEM used for the computation study. In the context of a chemical mixture, the RSD% for the molar composition was minimized by adjusting the molecular energy and size parameters, k_{ij} and η_{ij}, respectively. This adjustment was made to optimize the accuracy of predicting the behavior of the mixture. The purpose of the investigation was to study the temperature dependence of the energy parameter, which is an essential factor in determining the properties of such mixtures at different temperatures. The study aimed to furnish perception into the behavior of the mixture under different conditions and to help improve the precision of modeling chemical mixtures.

The accurate correlation of VLE can be achieved by employing mixing rules and a cubic EOS. The precision of pure compound vapor pressure data representation is crucial for this purpose. The model coefficients, P-R constants a and b, are responsible for molecular interactions and can be predicted using statistical thermodynamics and mixing rules. A conventional one-binary parameter mixing rule is appropriate for most systems, but for binary systems containing polar compounds and saturated hydrocarbons, the two-binary parameter mixing rule is vital [57, 58]. Furthermore, for binary systems involving saturated hydrocarbons and highly asymmetric mixtures, a composition-dependent two-binary-parameter mixing rule for the P-R equation leads to a significant enhancement in the fit quality of VLE data. Utilizing a second-order mixing rule for constants a and b is essential for capturing concentration-dependent changes and accurately representing non-ideal behavior in complex binary mixtures.

To predict the phase diagram, 15 datasets for the 3C2HM component system and 13 datasets for the 2NMEM system were analyzed at a temperature of 353.2 K. Figure 4a and 4b shows the pressure vs. mole fraction plots comparing the measured data of $CO_2 + 3C2HM$ and $CO_2 + 2NMEM$ with P-R EOS modeling at 353.2 K. In the graphs, the blue broken curves represent the results of zero IPs, whereas the red solid line with symbols represents the results with fitted non-zero IPs. The isotherm at 353.2 K for both systems explains the impact of composition and pressure on the phase transition points and follows the simplest Type I category, which is consistent with the results presented in Figs. 3a and 3b. The optimized molecular IPs of the $CO_2 + 3C2HM$ system isotherm ($T = 353.2$ K) were estimated to be $k_{ij} = 0.000$ and $\eta_{ij} = -0.045$, while those of the $CO_2 + 2NMEM$ system

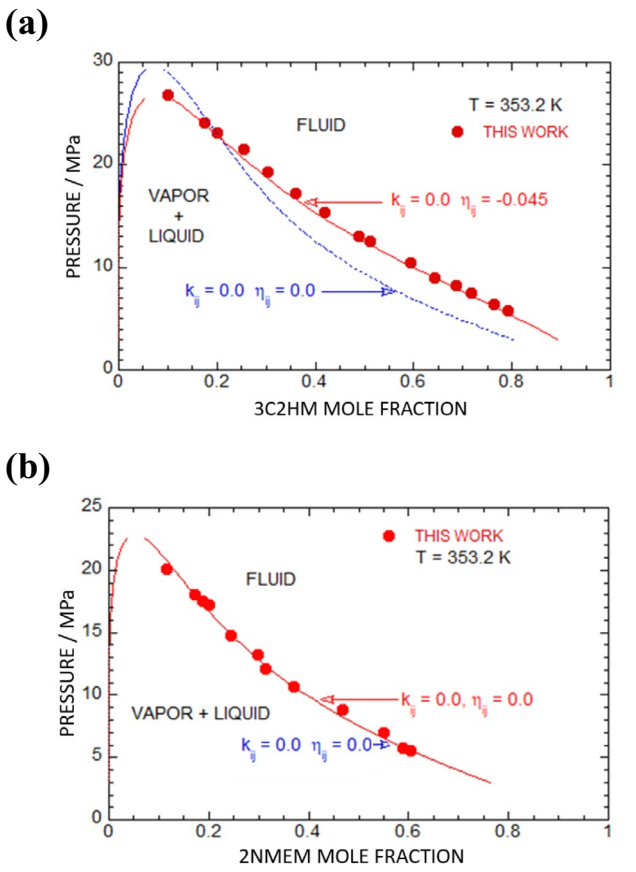

Fig. 4 Pressure *vs.* mole fraction plots comparing the experimental data (solid symbols) of the $CO_2 + 3C2HM$ $\{(1-x)CO_2 + x\ H_2C=C(CH_3)CO_2CH_2CH(OH)CH_2Cl\}$ (a) and $CO_2 + 2NMEM$ $\{(1-x)CO_2 + x\ H_2C=C(CH_3)CO_2(CH_2)_2C_4H_8NO\}$ (b) systems with the calculation results obtained using the P-R EOS equation of state with $k_{ij} = 0.000$ and $\eta_{ij} = -0.045$ [$CO_2 + 3C2HM$ **a**] and $k_{ij} = 0.000$, $\eta_{ij} = 0.000$ [$CO_2 + 2NMEM$ **b**] at 353.2 K. Blue broken curves refers to the results of zero interaction parameters whereas red solid line with symbols represents the results with fitted non-zero interaction parameters

isotherm were $k_{ij} = 0.000$ and $\eta_{ij} = 0.000$. The plots demonstrate that the IPs of the cubic EOS fit well with the measured VLE dataset at 353.2 K. The isotherm predicted with the IPs explains the ideal behavior of two-component systems [59–61].

For instance, zero values of the k_{ij} parameter indicate the ideal behavior of the pure component binary systems, whereas a positive or negative sign of the IPs indicates the nonideality of the solution. The results presented in Fig. 4a confirm that the $CO_2 + 3C2HM$ binary system is nonideal, as the zero-result blue-colored curve deviates from the experimental non-zero result curve. Hence, it requires specific parameters to describe the phase behavior. Additionally, the negative sign of the IPs indicates that there is a repulsive force between the solution molecules, and this force is different for each molecule. Conversely, the zero-result curve and

non-zero-result curve of the $CO_2 + 2NMEM$ system are well fitted, indicating that the system is ideal. This is supported by the positive sign of the magnitude of the IPs. Therefore, we can conclude that the molecular interaction between CO_2 and 2NMEM as well as CO_2 and 3C2NM were variable. In both systems, the boundary between the single-phase region and the two-phase vapor–liquid region is clearly defined by the red solid line, with the former being above and the latter being below the line. This is a well-established and widely accepted concept in the phase diagram. Consequently, we can practically fit the experimental result and correlation results by evaluating the IPs obtained at the temperature of 353.2 K for both systems. Additionally, the optimized molecular IPs were nearly zero, indicating that both binary systems are nearly ideal mixture systems.

Comparison of the Experimental with Modeled VLEs

The experimental laboratory VLE dataset was correlated with the data predicted using the model (P-R EOS). The model data was obtained by optimizing the IPs at a temperature of 353.2 K and predicting the isotherms for both binary systems at five various temperatures. Figures 5a and 5b show the results of the comparison of the measured data and the model prediction for the $CO_2 + 3C2HM$ and $CO_2 + 2NMEM$ systems, respectively. The model prediction for the 3C2HM monomer system was evaluated based on the magnitude of the energy parameter of $k_{ij} = 0.000$ and the size parameter of $\eta_{ij} = -0.045$. Similarly, the model isotherms for the 2NMEM system were predicted based on the magnitude of the energy parameter of $k_{ij} = 0.000$ and the size parameter of $\eta_{ij} = 0.000$. Figure 5b shows that the model-predicted isotherms accurately fit the experimental isotherms since the IP values were zero. Thus, the predicted phase behavior matched well with the laboratory phase transitions of the $CO_2 + 2NMEM$ system under wide T, P, and x ranges of $313.2 \le T \le 393.2$ K, $3.25 \le P \le 28.70$ MPa, and $0.0560 \le x \le 0.6037$, respectively. However, the model-predicted isotherms for the $CO_2 + 3C2HM$ system did not fit well with all the experimental isotherms, as shown in Fig. 5a. Among the different isotherms, only the isotherms evaluated at 313.2 K and 333.2 K deviated from the recorded data. Hence, further evaluation was conducted to reduce the RSD%.

Figure 6 illustrates the model prediction error reduced using the IPs and a correlation of the experimental data for the $CO_2 + 3C2HM$ system. The outcomes of this comparison are presented in a concise and clear manner, highlighting the effectiveness of the model prediction. When Figs. 5a and 6 are compared, it can be seen that all the recorded isotherms shown in Fig. 6 that were studied at different temperatures perfectly match the P-R EOS computation under the reduced RSD% obtained by adjusting the IPs at each temperature.

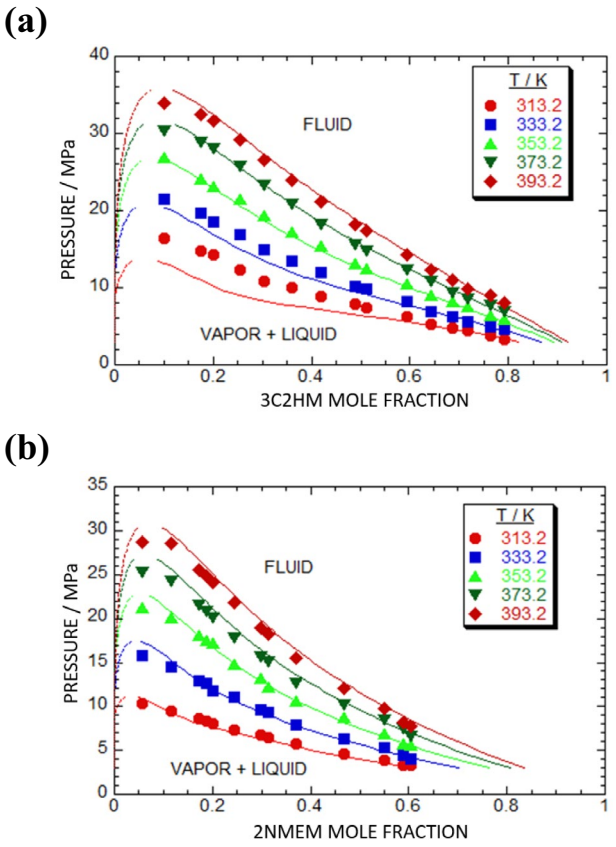

Fig. 5 Comparison of experimental vs. predicted isotherm plots of the $CO_2 + 3C2HM$ $\{(1-x)CO_2 + x\ H_2C=C(CH_3)CO_2CH_2CH(OH)CH_2Cl\}$ **a** and $CO_2 + 2NMEM$ $\{(1-x)CO_2 + x\ H_2C=C(CH_3)CO_2(CH_2)_2C_4H_8NO\}$ **b** systems with the calculation results obtained using the P-R EOS correlation at 353.2 K. Solid symbols refer to the experimental data points at various temperature whereas solid curves are predicted isotherms

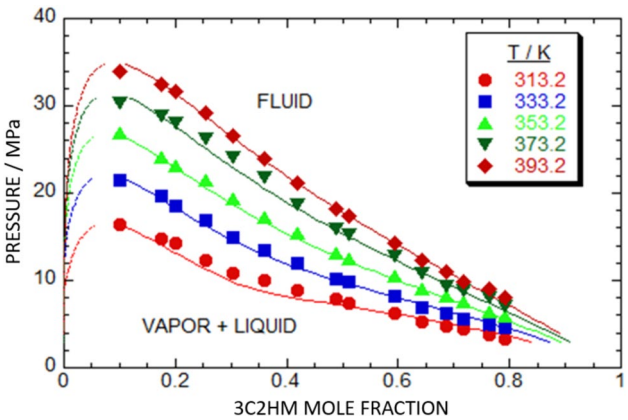

Fig. 6 Comparison of experimental data for the $CO_2 + 3C2HM$ $\{(1-x)CO_2 + x\ H_2C=C(CH_3)CO_2CH_2CH(OH)CH_2Cl\}$ (solid symbols.) system with the results of P-R EOS model calculated data (solid curves) with the adjusted k_{ij} and $\eta_{ij.}$ parameters to reduce RSD% at various selected temperature ●, 313.2.K; ■, 333.2.K; ▲, 353.2.K; ▼, 373.2.K; ◆, 393.2.K

Thus, the predicted phase behavior fits well with the experimental phase transitions of the $CO_2 + 3C2HM$ system under wide T, P, and x ranges of $313.2 \le T \le 393.2$ K, $3.36 \le P \le 33.90$ MPa, and $0.1002 \le x \le 0.6037$, respectively. Thus, the P-R EOS model containing the optimized molecular IPs at 353.2 K accurately predicted the solution phase behavior related to Type I simple behavior. The model shows a high level of accuracy in predicting the VLE for both binary mixtures, as the results are in good agreement with the recorded results. Similarly, many reports have confirmed the ability of the P-R EOS model to predict the phase diagram for different pure component binary systems [62–64].

Theoretical Computation Precision Critique

The experimental VLE data was correlated utilizing the thermodynamic model with the averaged k_{ij} and η_{ij} parameters evaluated at 353.2 K. The IPs were evaluated to compute the VLE dataset for the $CO_2 + 3C2HM$ and $CO_2 + 2NMEM$ systems across all temperature and pressure ranges. For each temperature, 15 and 13 data points were considered for the $CO_2 + 3C2HM$ and $CO_2 + 2NMEM$ systems, respectively. The validity of the P-R EOS model was assessed using the RSD%. Table 5 presents the effect of two independent parameters on the RSD% for each isotherm of both systems. The RSD% of the $CO_2 + 3C2HM$ system employing the optimized IPs ($k_{ij} = 0.000$ and $\eta_{ij} = -0.045$) was 17.98%, 7.07%, 3.06%, 2.41%, and 3.86% at temperatures of 313.2, 333.2, 353.2, 373.2, and 393.2 K, respectively. The calculated average RSD% was 8.98%, indicating that the model values are poorly fitted with the experimental data, particularly for the isotherms evaluated at 313.2 K (17.98%) and 333.2 K (7.07%). To improve the RSD%, the magnitude of the energy parameter of k_{ij} (at constant $\eta_{ij} = -0.045$) was adjusted as a function of temperature in the $CO_2 + 3C2HM$ system. The values of the energy parameters of the system were nearly zero and decreased as the temperature increased, and the average RSD% reduced from the previous estimation (Fig. 7). Thus, it can be inferred that the energy and key parameters are temperature-dependent parameters [65, 66].

Binary systems can become a nearly ideal mixture system as the temperature increases. The accuracy of the prediction of the optimized energy parameters was tested using regression analysis, and the reasonable regression coefficient (R^2) was found to be 0.97701 (≥ 0.95), confirming the precision of the prediction. Based on the re-optimized IPs, the RSD% of the $CO_2 + 3C2HM$ system was found to be 7.87%, 3.27%, 3.12%, 4.14%, and 3.30% at temperatures of 313.2, 333.2, 353.2, 373.2, and 393.2 K, respectively. The calculated average RSD% was found to be 4.70%, indicating that the model values fit the experimental data reasonably. This claim is in concordance with Fig. 6, which shows the plotted results obtained from the reduced average error. Surprisingly, the average RSD% for the $CO_2 + 2NMEM$ system employing the optimized IPs ($k_{ij} = 0.000$ and $\eta_{ij} = 0.000$) was calculated to be 4.91%, and the RSD% for each isotherm was estimated to

Table 5 The effect of two binary interaction parameters on the percentage of RSD for each isotherm of $CO_2 + 3$-chloro-2-hydroxypropyl methacrylate (3C2HM) and $CO_2 + 2$-*N*-morpholinoethyl methacrylate (2NMEM) systems

Mixture	Binary interaction parameters		N	*T*/K	RSD%
	k_{ij}	η_{ij}			
$CO_2 + 3C2HM$	0.000	− 0.045	15	313.2	17.98
			15	333.2	7.07
			15	353.2	3.06
			15	373.2	2.41
			15	393.2	3.86
					8.98
	0.012	− 0.045	15	313.2	7.87
	0.005	− 0.045	15	333.2	3.27
	− 0.009	− 0.045	15	353.2	3.12
	− 0.007	− 0.045	15	373.2	4.14
	− 0.005	− 0.045	15	393.2	3.30
					4.70
$CO_2 + 2NMEM$	0.000	0.000	13	313.2	6.12
			13	333.2	4.10
			13	353.2	3.44
			13	373.2	5.13
			13	393.2	5.33
					4.91

k_{ij} energy parameter, η_{ij} key parameter, T_b: Boiling temperature, *N* Number of experimental runs, *T* Experimental temperature; *RSD%* root mean square deviation %

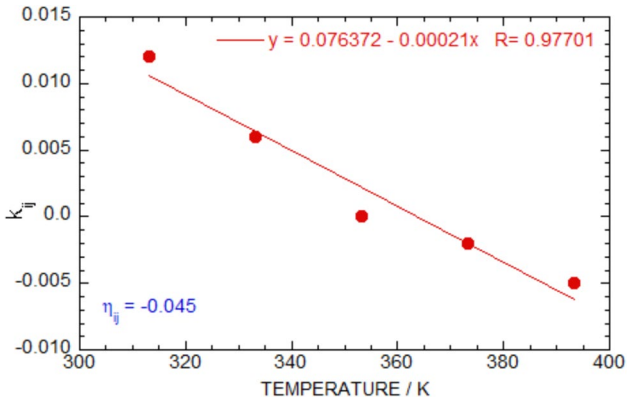

Fig. 7 Effect of k_{ij} parameter in the function of temperature at $\eta_{ij} = -0.045$ for the $CO_2 + 3C2HM$ $\{(1-x)CO_2 + x\ H_2C{=}C(CH_3)CO_2CH_2CH(OH)CH_2Cl\}$ system, estimated through P-R EOS model. Red Solid symbols refers to the energy (k_{ij}) parameter. Solid lines indicates that the effect of linear regression on the interaction parameters *vs.* temperature

be 6.12%, 4.10%, 3.44%, 5.13%, and 5.33% at temperatures of 313.2, 333.2, 353.2, 373.2 and 393.2 K, respectively. It should be noted that the P-R EOS-predicted VLE data paired perfectly with the measured values for the $CO_2 + 2NMEM$ system at the first attempt. Therefore, the average RSD% accurately critiques the precision of the prediction for the theoretical computational P-R EOS model. Based on the average RSD% values, it can be concluded that the optimized IPs employing the thermodynamic model prediction strongly fit the experimental phase behavior of both binary systems containing monomers in supercritical CO_2. Similar to this study, some previous studies have validated several phase diagram theoretical models for different binary systems using average RSD% [67–69].

Typical Characteristics of the Critical Solution Curve

Figure 8a and 8b depicts a typical critical solution curve of the experimental records and model computational dataset for the $CO_2 + 3C2HM$ [x $H_2C=C(CH_3)CO_2(CH_2)_2C_4H_8NO + (1-x)$ CO_2] and $CO_2 + 2NMEM$ [x $H_2C=C(CH_3)CO_2(CH_2)_2C_4H_8NO + (1-x)$ CO_2] systems. The simulated critical solution curves (P *vs.* T) display Type I phase behavior and provide useful information on the solubility and interactions of the chemical mixtures. The coexistence space (CLP) of the two-component systems was recorded at elevated pressure and temperature conditions. In the diagram, the solid red lines indicate the VLE lines, while the red solid circles indicate the CLP of the pure components of the mixtures. The blue dashed curve represents the P-R EOS-predicted critical curve obtained at different temperatures, and the blue solid squares represent the CLP of the binary mixture determined from the isotherm experiments.

The CLP for the pure components of CO_2 (T_c: 304.2 K and P_c: 7.38 MPa), 3C2HM (T_c: 776.9 K and P_c: 3.45 K), and benzyl acetate (T_c: 772.6 K and P_c: 2.79 MPa) compounds were extended toward the critical solution curve to satisfy the VLE of both binary systems. The bottom of the critical solution curve for both systems represents the two-phase region of the vapor-to-liquid phase, while the overhead of the curve represents the single-phase (vapor–liquid) fluid region, which appears throughout the phase diagram [70, 71]. The vapor pressure and critical points of the pure components were determined using the Lee–Kesler method and the Joback and Lydersen method, respectively. The critical pressure point for the $CO_2 + 3C2HM$ system was found to be 33.90 MPa at 393.2 K, while those for the $CO_2 + 2NMEM$ system were 20.07 MPa at 353.2 K and 20.86 MPa at 373.2 K, and these points were recorded when the one-phase region was reached. None of the examined isotherms of the binary systems exhibited three-phase behavior. In conclusion, the typical critical solution curves provide useful insights into the phase transition behavior of the mixture of

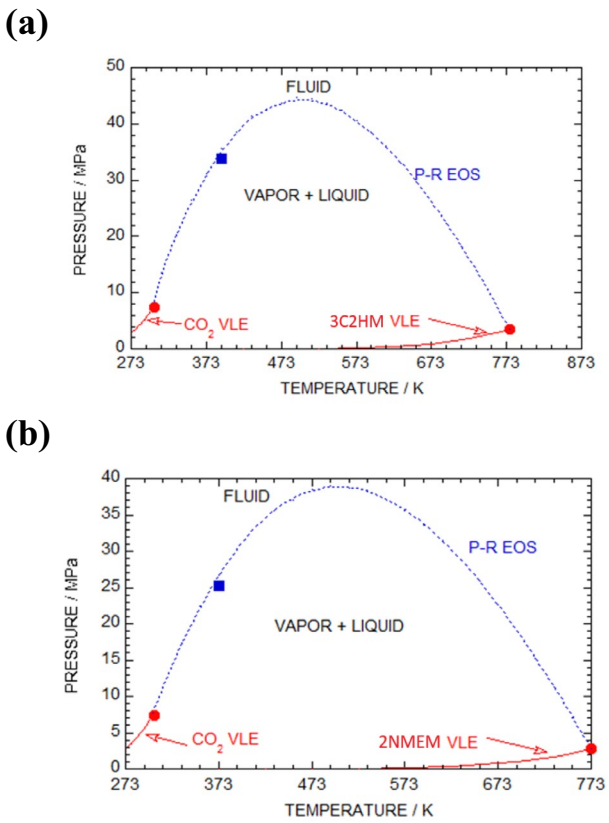

Fig. 8 Pressure vs. temperature space plots for the $CO_2 + 3C2HM$ $\{(1-x)CO_2 + x$ $H_2C=C(CH_3)CO_2CH_2CH(OH)CH_2Cl\}$ **a** and $CO_2 + 2NMEM$ $\{(1-x)CO_2 + x$ $H_2C=C(CH_3)CO_2(CH_2)_2C_4H_8NO\}$ **b** systems. Solid curves denote the vapor–liquid equilibrium curves, whereas red solid circles represent critical points for pure CO_2, 3C2HM and 2NMEM compounds. Mixture critical points, denoted by blue solid squares, were determined from the isotherm experiment. Dashed curves (blue) represent the calculation results obtained using P-R EOS model with optimized IPs

monomers in CO_2 and can be used to determine the thermodynamic properties of two-component systems.

Conclusion and Outlook

In this study, the phase diagrams for two-component systems, namely, $CO_2 + 3C2HM$ and $CO_2 + 2NMEM$, were examined over a wide range of conditions, including $313.2 \le T \le 393.2$ K, $3.25 \le P \le 33.90$ MPa, and $0.0560 \le x \le 0.7925$. It was discovered that the rise in temperature under constant pressure, the amount of CO_2 that can dissolve in the liquid phase of the monomer decreases. The binary systems follows the Type I solution phase behavior and had nearly identical phase diagrams. The 2NMEM component exhibited higher polarizability and lower surface tension than the 3C2HM monomer, making it less soluble in CO_2 since CO_2 is a nonpolar compound. The phase

diagram was not affected by changes in the chemical configuration of the two monomers, but the phase transition conditions changed because of the molecular interactions between CO_2 and the monomer. The measured data for the binary systems were strongly correlated with the P-R EOS thermodynamic model. For the isotherm ($T = 353.2$ K), the optimized molecular IPs of the $CO_2 + 3C2HM$ system were estimated to be $k_{ij} = 0.000$ and $\eta_{ij} = -0.045$, while those of the $CO_2 + 2NMEM$ system were $k_{ij} = 0.000$ and $\eta_{ij} = 0.000$. As a result, the phase diagram of the $CO_2 + 3C2HM$ and $CO_2 + 2NMEM$ systems were similar whereas the molecular interactions between CO_2 and 3C2HM and CO_2 and 2NMEM were variable. Changes in the chemical configuration of the monomer did not affect the phase diagram, however, it affected the interaction between CO_2 and the monomer thus influencing the ideal behavior of the systems. Furthermore, the optimized molecular IPs were nearly zero, confirming that both binary systems are nearly ideal mixture systems as the temperature increases.

The predicted phase behavior matched well with the laboratory phase transitions of both systems. The average RSD% accurately critiques the precision of the prediction for the theoretical computational P-R EOS model. The calculated average RSD% for the $CO_2 + 3C2HM$ and $CO_2 + 2NMEM$ system was found to be 4.70% and 4.91%, respectively, indicating that the model values are a reasonable fit. The simulated characteristics of the critical solution curve (P vs. T) clarified the interactions and transitions of the studied binary systems. Moreover, the solubility analysis is suitable for industrial settings and provides significant insights into the phase behavior of methacrylate binary systems under various operating conditions. The findings of the present study have important implications for upcoming study in this field and will undoubtedly contribute to the evolution of highly accurate and reliable models for predicting the behavior of chemical systems.

Acknowledgements This work was supported by the National Research Foundation of Korea (NRF) grant funded by the Korean government (MSIT) (No. 2021R1A2C2006888).

Data availability Data will be made available upon request.

Declarations

Conflict of interest The authors declare that they have no known competing financial interests or personal relationships that could have appeared to influence the work reported in this paper.

References

1. S. Son, J.I. Lee, Nucl. Eng. Technol.. Eng. Technol. **56**, 1254 (2024)
2. F.J.G. Ortiz, A. Kruse, React. Chem. Eng. **5**, 424 (2020)
3. H. Park, J.S. Kim, S. Kim, E.S. Ha, M.S. Kim, S.J. Hwang, Pharmaceutics **13**, 1928 (2021)
4. Z. Liu, R. Navik, H. Tan, Q. Xiang, M. Goto, R.M. Ibarra, Y. Zhao, J. Supercrit. FluidsSupercrit. Fluids **188**, 105672 (2022)
5. I. Khmelinskii, L.V. Woodcock, Entropy **22**, 437 (2020)
6. J. Xu, Y. Wang, X. Ma, Phys. Rev. E **104**, 014142 (2021)
7. Y.K. Tovbin, Russ. J. Phys. Chem. **17**, 1569 (2023)
8. F.S.A. Razzak, J. Sci. Res. **65**, 1 (2021)
9. P. Nikolai, B. Rabiyat, A. Aslan, A. Ilmutdin, J. Therm. Sci. **28**, 394 (2019)
10. C Campalani, E Amadio, S Zanini, S Dall Acqua, M Panozzo, S Ferrari, A Perosa. 2020. Sfgg. J Util. 41 101259.
11. Y. Gao, D. Zhou, J. Lyu, Q. Xu, B. Newland, K. Matyjaszewski, W. Wang, Nat. Rev. Chem. **4**, 194 (2020)
12. A.P. Fugolin, S. Lewis, M.G. Logan, J.L. Ferracane, C.S. Pfeifer, Dent. Mater. J. **36**, 1028 (2020)
13. P.V. Kelly, P. Cheng, D.J. Gardner, W.M. Gramlich, Macromol. Rapid Commun.. Rapid Commun. **42**, 2000531 (2021)
14. E.I. Muresan, G. Rosu, A. Danila, M. Drobota, F. Doroftei, C.D. Radu, J. Eng. Fibers Fabr.Fabr. **14**, 1558925019851340 (2019)
15. V. Malshe, M. Vaidya, React. Funct. Polym.Funct. Polym. **39**, 83 (1999)
16. -Chloro-2-Hydroxypropyl Acrylate, http://www.chemspider.com/Chemical-Structure.83910.html.
17. X. Peng, F. Du, L. Zhong, Synthesis, characterization, and applications of hemicelluloses based eco-friendly polymer composites, in *Sustainable Polymer Composites and Nanocomposites*. ed. by S. Kumar, R. Mishra, A. Asiri (Springer, Cham, 2019)
18. J. Eichhorn, M. Klein, I. Romanenko, F.H. Schacher, Polym. Chem.. Chem. **13**, 4421 (2022)
19. -N-Morpholinoethyl Methacrylate. https://www.sigmaaldrich.com/KR/ko/product/aldrich/729833.
20. M.N. Leshina, N.Y. Ladilova, A.A. Malysheva, Russ. J. Appl. Chem. **91**, 1118 (2018)
21. F. Faraguna, R. Blažic, E. Vidović, A. Jukić, React. Funct. Polym. Funct. Polym. **177**, 105315 (2022)
22. M.A. McHugh, F. Rindfleisch, P.T. Kuntz, C. Schmaltz, M. Buback, Polymer **39**, 6049 (1998)
23. J. Jennings, S.P. Bassett, D. Hermida-Merino, G. Portale, W. Bras, L. Knight, S.M. Howdle, Polym. Chem.. Chem. **7**, 905 (2016)
24. D.W. Cho, J.H. Lee, J. Shin, W. Bae, H. Kim, M.S. Shin, J. Chem. Thermodyn.Thermodyn. **43**, 1666 (2011)
25. M. Lora, M.A. McHugh, Fluid Phase Equilib.Equilib. **157**, 285 (1999)
26. H.S. Byun, H.Y. Lee, J. Chem. Eng. Data **51**, 1436 (2006)
27. S.H. Cho, B.S. Lee, H.S. Byun, J. CO2 Util. **25**, 39 (2018)
28. D. Dhamodharan, M.S. Park, S. Mubarak, H.S. Byun, Arab. J. Chem. **16**, 104862 (2023)
29. U.S. Behera, S.K. Prasad, H.S. Byun, J. Mol. Liq. **393**, 123553 (2024)
30. P.N. Ghoderao, H.S. Byun, J. Mol. Liq. **397**, 124067 (2024)
31. H.S. Byun, C. Park, Korean J. Chem. Eng. **19**, 126 (2002)
32. S.D. Yoon, H.S. Byun, J. Chem. Thermodyn.Thermodyn. **71**, 91 (2014)
33. H.S. Byun, K. Kim, M.A. McHugh, Ind. Eng. Chem. Res. **39**, 4580 (2000)
34. P.N. Ghoderao, D. Dhamodharan, H.S. Byun, J. Chem. Thermodyn.Thermodyn. **168**, 106746 (2022)
35. H.S. Byun, M.Y. Choi, J.S. Lim, J. Supercrit. FluidsSupercrit. Fluids **37**, 323 (2006)
36. D. Dhamodharan, C.W. Lee, H.S. Byun, New J. Chem. **47**, 4043 (2023)
37. P.N. Ghoderao, D. Dhamodharan, S. Mubarak, H.S. Byun, J. Mol. Liq. **358**, 119131 (2022)
38. E.P. Bruce, J.M. Prausnitz, *The properties of gases and liquids* (McGraw-Hill, New York, 2001)

39. Y. Nannoolal, J. Rarey, D. Ramjugernath, W. Cordes, Fluid Phase Equil. **226**, 45 (2004)
40. Y. Nannoolal, J. Rarey, D. Ramjugernath, Fluid Phase Equil. **252**, 1 (2007)
41 K.S. Pitzer, D.Z. Lippmann, C.M. Huggins, D.E. Petersen, Volumetric thermodyn. Prop. Fluids **77**, 3433 (1955)
42. J.P. Mize, *Optimization techniques with FORTRAN* (McGraw-Hill, Inc, 1973)
43. J.L. Fulton, G.G. Yee, R.D. Smith, J. Am. Chem. Soc. **113**, 8327 (1991)
44. H.A. Patel, S. Hyun Je, J. Park, D.P. Chen, Y. Jung, C.T. Yavuz, Nat. Commun.Commun. **4**, 1357 (2013)
45. Y.T. Kwon, D. Dhamodharan, H. Choi, S.W. Shim, H.S. Byun, Korean J. Chem. Eng. **39**, 2783 (2022)
46. D. Dhamodharan, P.P. Ghoderao, H.S. Byun, J. Mol. Liq. **357**, 119112 (2022)
47. H.S. Lee, P.N. Ghoderao, M.S. Park, H.S. Byun, J. Mol. Liq. **387**, 122651 (2023)
48. C.W. Park, C.H. Kim, H.S. Byun, Korean J. Chem. Eng. **38**, 610 (2021)
49. S. Zid, J.P. Bazile, J.L. Daridon, A. Piña-Martinez, J.N. Jaubert, S. Vitu, J. Supercrit. FluidsSupercrit. Fluids **179**, 105387 (2022)
50. P.H. Van Konynenburg, R.L. Scott, Philos Tr. Roy. Soc. London. Series A **298**, 495 (1980)
51. M. da Ponte, Phys. Chem. Chem. Phys. **1**, 5369 (1999)
52. E. Aionicesei, M. Škerget, Z. Knez, J. Chem. Eng. Data **53**, 185 (2008)
53. Y. Marcus, J. Supercrit. FluidsSupercrit. Fluids **38**, 7 (2006)
54. A.G. Perez, C. Coquelet, P. Paricaud, A. Chapoy, Fluid Phase Equilib.Equilib. **440**, 19 (2017)
55. J.C. Tsai, Y.P. Chen, Fluid Phase Equil. **145**, 193 (1998)
56. F.A. Perdomo, S.H. Khalit, E.J. Graham, F. Tzirakis, A.I. Papadopoulos, I. Tsivintzelis, A. Galindo, Fluid Phase Equil. **566**, 113635 (2023)
57. R. Stryjek, J.H. Vera, R. Stryjek, J.H. Vera, Can. J. Chem. Eng. **67**, 523 (1989)
58. A. Piña-Martinez, R. Privat, I.K. Nikolaidis, I.G. Economou, J.N. Jaubert, Ind. Eng. Chem. Res. **60**, 17228 (2021)
59. D. O'Hanlo, R.J. Forster, Langmuir **16**, 702 (2000)
60. J.N. Jaubert, R. Privat, Fluid Phase Equil. **295**, 26 (2010)
61. S.H. Mushrif, A.V. Phoenix, Ind. Eng. Chem. Res. **47**, 6280 (2008)
62. P.N. Ghoderao, C.W. Lee, H.S. Byun, J. Mol. Liq. **372**, 121206 (2023)
63. J.H. Yim, Y.S. Choo, H.S. Byun, J. Chem. Thermodyn.Thermodyn. **130**, 140 (2019)
64. P.N.P. Ghoderao, M. Narayan, V.H. Dalvi, Korean J. Chem. Eng. **39**, 3452 (2022)
65. H. Matsukawa, Y. Shimada, S. Yoda, Y. Okawa, M. Naya, A. Shono, K. Otake, Fluid Phase Equil. **455**, 6 (2018)
66. P.N. Ghoderao, C.W. Lee, H.S. Byun, J. Ind. Eng. Chem. **121**, 92 (2023)
67. G. Yang, Z. Fan, X. Li, Chem. Eng. J. **378**, 122032 (2019)
68. Y. Bakhbakhi, Math. Comput. Model.Comput. Model. **55**, 1932 (2012)
69. W. Gao, R.L. Robinson, K.A. Gasem, J. Chem. Eng. Data **44**, 130 (1999)
70. P.N. Ghoderao, J. Kim, H.S. Byun, Ind. Eng. Chem. Res. **62**, 21428 (2023)
71. H.S. Byun, P.N. Ghoderao, H.S. Lee, M.S. Park, Arab. J. Chem. **16**, 105290 (2023)